THE ASTROPHYSICAL JOURNAL, 418:L75–L78, 1993 December 1

MOLECULAR HYDROGEN IN THE IRAS 03282+3035 STELLAR JET

JOHN BALLY[1] AND DAVID DEVINE[2]
Department of Astrophysical, Planetary, and Atmospheric Sciences, and Center for Astrophysics and Space Astronomy, Campus Box 389, University of Colorado, Boulder, CO 80309

AND

MARK HERELD[3] AND BERNARD J. RAUSCHER[4]
Department of Astronomy and Astrophysics, The University of Chicago, 5640 South Ellis Avenue, Chicago, IL 60637
Received 1993 August 20; accepted 1993 September 17

ABSTRACT

We detected shock-excited 2.122 μm molecular hydrogen from the blueshifted lobe of the highly collimated CO outflow associated with the young stellar object IRAS 03282+3035 in the Perseus molecular cloud. The H_2 emission has a peak surface brightness of 5×10^{-4} ergs s^{-1} cm^{-2} sr^{-1}, making this one of the brightest shock-excited molecular hydrogen sources associated with a low-mass young stellar object. The emission has knotty structure with faint tails lying parallel to the mean outflow axis. These knots coincide with molecular "bullets" B3 and B4 located near the end of the highest velocity CO-emitting component and may be bow shocks where a fast jet interacts with the surrounding medium. The bulk of the lower velocity CO emission is located downwind from the H_2 emission zone. We discuss the complex morphology in the context of jet-driven CO outflow models and argue that the H_2 emission delineates regions where CO-bearing gas is entrained in the flow and accelerated, thereby producing the more slowly moving CO outflow. The H_2 luminosity radiated by this outflow is about 10% of the bolometric luminosity of the central driving source. This is the largest ratio of the $L(H_2)/L_{bol}$ for any known young stellar object.

Subject headings: infrared: interstellar: lines — ISM: jets and outflows — ISM: molecules — stars: formation — stars: individual (IRAS 03282+3035) — stars-pre–main-sequence

1. INTRODUCTION

In bipolar outflows from young stellar objects (YSOs), molecular hydrogen lines at 2 μm trace shocks propagating into dense ($n > 10^4$ cm^{-3}) molecular gas and can be used to study the structure of the outflow with subarcsecond resolution. The morphology of shocks on these scales constrains outflow models. Masson & Chernin (1993), Raga et al. (1993), and Raga & Cabrit (1993) propose that bipolar outflows are swept up from the host cloud by the action of a bipolar jet from a YSO. In this *Letter* we provide evidence that shock-excited H_2 emission in the IRAS 03282+3035 outflow in Perseus (IRAS 0328 for short) traces the CO acceleration region in a bipolar outflow.

Recent studies show that the youngest YSOs are only visible at submillimeter and far-infrared wavelengths. These sources are frequently first detected by their bipolar CO outflows which are highly collimated, have large CO velocities (>100 km s^{-1}), and contain discrete high-velocity clumps ("molecular bullets"). Members of this class include NGC 2264G (Margulis et al. 1990), ρ-Oph-A (André et al. 1990), NGC 1333 HH 7-11 (Masson, Mundy, & Keene 1990; Bachiller & Cernicharo 1990), NGC 2024 (Richer, Hills, & Padman 1992), L1448 (Bachiller et al. 1990), and IRAS 0328 (Bachiller, Martín-Pintado, & Planesas 1991). All of these sources exhibit near-infrared emission from shock-excited H_2, except ρ-Oph-A, which may be too obscured.

At a distance of 350 pc (Borgman & Blaauw 1964), the Perseus molecular cloud is one of the best regions of the sky for the study of the detailed morphology of young stars and their outflows. The Perseus cloud contains a number of cloud cores such as B1, B5, L1448, and the core which contains IRAS 0328 in which isolated low-mass stars have recently formed (Bachiller & Cernicharo 1986a, b). Bally, Lada, & Lane (1993) presented detailed observations of the 2.122 μm H_2 $S(1)$ line from shocks in the L1448 bipolar CO outflow. In that source, there appears to be a correlation between strong H_2 emission and the location of 10^{-4} $M_\odot$ molecular "bullets" seen in CO and SiO emission lines. A similar relationship between bullets and H_2 emission is seen in NGC 1333 HH 7-11 (Garden, Russell, & Burton 1990).

IRAS 0328 is the third example of a CO bipolar molecular outflow in Perseus with molecular "bullets." Bachiller et al. (1991) show that the CO emission at the highest radial velocities ($|V|$ about 60 km s^{-1}) traces a highly collimated jet with a length to width ratio of more than 30. The CO jet "zig-zags" about the axis defined by the lower velocity CO emission. Four molecular "bullets" have been identified in the blueshifted CO lobe, and three are seen toward the redshifted lobe. We present near-infrared broad-band K and narrow-band observations of the 2.122 μm wavelength $S(1)$ line of H_2 toward the outflow lobes of IRAS 0328 and discuss implications of these data for models of molecular outflows.

2. OBSERVATIONS AND DATA REDUCTION

A mosaic of images was made on 1992 October 10 and 11 with the Apache Point Observatory telescope (operated by the Astrophysics Research Consortium—ARC), which at the time was using a 1.8 m diameter mirror on loan from the University of Calgary. We used the Apache Point Observatory's Near-Infrared GRism Spectrometer and IMager (GRIM), which is equipped with a liquid nitrogen–cooled 128 × 128 pixel

[1] E-mail: bally@janos.colorado.edu.
[2] E-mail: devine@casa.colorado.edu.
[3] E-mail: hereld@oddjob.uchicago.edu.
[4] E-mail: bjr@oddjob.uchichago.edu.

HgCdTe NICMOS2 detector sensitive to radiation between 1.2 and 2.6 μm (Hereld et al. 1993).

We took a series of 15 s exposures through a broad-band K filter and 240 s images through a narrow-band (1% passband) interference filter centered on the 2.122 μm $v = 1$–0 $S(1)$ line of molecular hydrogen. Both the narrow-band and broad-band observations covered the entire area of the sky over which the CO outflow is seen. Our mosaic extended over 5′ to the southeast and northwest of IRAS 0328 (whose epoch 1950 position was assumed to be $\alpha = 03^h28^m15^s.2$, $\delta = 30°35'14''$) and extends more than 2′ orthogonal to the CO outflow axis.

We used the Elias standard stars (Elias et al. 1982) HD 22686, HD 18881, and HD 40335 to calibrate the data taken with both filters. Analysis of the calibration data indicates variations of $\sim 5\%$ in the atmospheric transmission and in overall system gain. We estimate that our fluxes are uncertain by about $\pm 10\%$.

The flux ratio per unit exposure time in the broad-band to the narrow-band filters is about 20.7 ± 0.3 for HD 18881. If N is the number of counts in a pixel, and t the integration time in seconds, then for GRIM on the Apache Point 1.8 m telescope we find a total surface brightness $B = 4.81 \times 10^{-4} N/t$ (ergs s^{-1} cm^{-2} sr^{-1}) in the 2.122 μm filter, and a brightness per unit frequency interval $B_\nu = 1.34 \times 10^{-17} N/t$ (ergs s^{-1} cm^{-2} Hz^{-1} sr^{-1}) in the K-band filter. Our observations are complete to a K-band limiting magnitude of about 15 at the 3 σ level, averaged over the spatial extent of the seeing disk of a star.

The image scale was established by astrometry of stars in the globular cluster M92 and camera orientation on the sky was determined from the change in position of stars on the detector when the telescope was moved by a known amount. Each pixel subtends 0″.723 on the sky, and the array has a field of view of 93″ × 93″.

A median sky frame was computed from observations taken within a few hours of each "on-source" frame. A "flat" frame was then produced by subtracting a dark frame from the median sky and then normalizing the result. Sky frames were subtracted from individual "on" frames and then divided by the "flat." The resulting frames were adjusted to have a zero mean background level and placed into the final mosaic.

3. RESULTS

Figure 1 (Plate L7) a gray-scale representation of our 2.122 μm narrow-band (line + continuum) mosaic showing the full extent of the molecular hydrogen emission in the southeastern blueshifted CO outflow lobe. No emission was detected toward the redshifted CO lobe of the outflow. Any H_2 emission in the redshifted lobe may be too obscured by foreground material to be seen at 2 μm. Furthermore, no emission was seen in either the 2.122 μm or the K filter from the vicinity of IRAS 0328 to a limiting surface brightness of 1.0×10^{-5} (ergs s^{-1} cm^{-2} sr^{-1}). We conclude that the exciting source of this outflow must be fainter than $m(K) = 15$ mag in the K band. This is consistent with the flux limits of IRAS 0328 at 12 and 25 μm and with the nondetection reported by Aspin (1992).

The flux observed in the K-band filter indicates that all of the diffuse emission shown in Figure 1 consists of shock-excited molecular hydrogen emission. Only two stars are seen near the bottom of Figure 1, and they have a flux ratio (flux in the K filter divided by flux in the 2.122 μm filter) of about 20. The diffuse emission has a flux ratio of about 3, indicating that there is about 3 times more emission in the K filter than in the narrow-band filter. This is consistent with pure shock-excited H_2 emission at an excitation temperature of about 2500 K. Thus, there is no evidence for reflection nebulosity from IRAS 0328 in our images.

Table 1 lists the surface brightness and other properties of the knots of H_2 emission seen in this source. Figure 2 shows a contour map of H_2 emission along with the regions over which the surface brightness was integrated to get the flux values given in Table 1. The numbers in column (1) correspond to the numbered boxes in Figure 2. Columns (2) and (3) lists the approximate R.A. and Decl. of the points of highest intensity in Figures 1 and 2. Column (4) gives the area-integrated fluxes (in instrumental units). Columns (5) and (6) give the area of each box in steradians and pixels. Column (7) gives the total flux received from each labeled region in Figure 2. Column (8) gives the isotropic H_2 $S(1)$ line luminosity assuming a distance of 350 pc. Finally, column (9) gives a corrected source luminosity for each region. We assume that the total H_2 luminosity from each

TABLE 1

IRAS 03282+3035 H_2 EMISSION

Clump (1)	R.A. 03^h28^m (2)	Decl.[a] 30°34′ (3)	I[b] ($\times 10^{-8}$) (4)	Area ($\times 10^{-9}$) (sr) (5)	Area[c] (pixel) (6)	Flux[d] ($\times 10^{-14}$) (ergs s^{-1} cm^{-2}) (7)	$L(2.122)$[e] ($\times 10^{31}$) (ergs s^{-1}) (8)	$L(H_2)$[f] ($L_\odot$) (9)
0[g]	...	...	88.1	69.7	5667	176	2.58	0.16
1	26.3	05″	44.9	12.1	984	90	1.33	0.083
2	24.2	01	13.4	9.22	750	27	0.39	0.025
3	23.7	45	6.22	8.50	691	12	0.18	0.011
4	26.8	−15	4.08	3.65	297	8	0.11	0.007
5	29.8	−43	2.31	3.86	314	5	0.07	0.004
Total	...	...	90.4	73.6	5984	181	2.66	0.166

[a] R.A. is in seconds, Decl. in arcseconds. The coordinates of the *IRAS* source are taken as R.A. = ($3^h28^m15^s.2$) and Decl. = (+30°35′14″.0). The central coordinates of the brightest emission in each region are listed and are accurate to about 5″.

[b] I is in average raw counts per pixel integrated over the boxes shown in Fig. 2 and has units of counts per pixel × sr.

[c] The image scale is 0.723 ± 0.001 arcsec pixel^{-1}.

[d] Flux based on the calibration formula given in the text. $F = 4.81 \times 10^{-4}\, I/t_{\rm int}$.

[e] The $S(1)$ line intensity, given by $L(2.122) = 4\pi d^2 F$, with $d = 350$ pc (Borgman & Blaauw 1964).

[f] $L(H_2) = fL(2.122) \times 10^{A_{2.2}/2.5}$ where $f \sim 10$ is the partition function for H_2(total)/H_2 $S(1)$ appropriate for a 2500 K shock-excited gas (Scoville et al. 1982) and $A_{2.2} \sim 1.0$ mag is the assumed extinction.

[g] Envelope of regions 1–4 (see Fig. 2).

PLATE L7

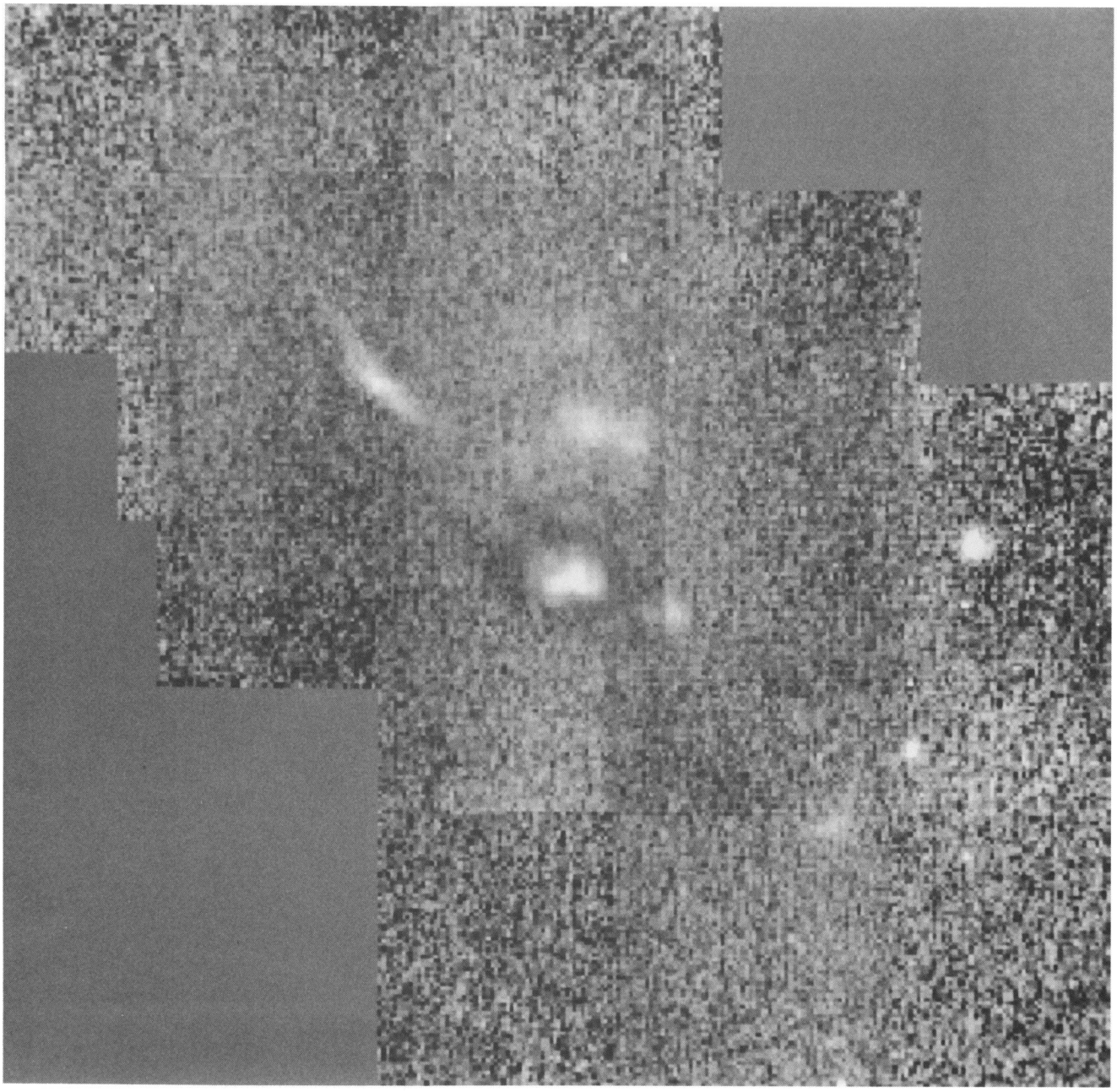

FIG. 1.—Gray-scale representation of the 2.122 μm $v = 1$–0 $S(1)$ H_2 line + continuum emission in the blueshifted lobe of the IRAS 03282+3035 molecular outflow. Although searched, no emission was found toward the redshifted lobe.

BALLY et al. (see 418, L76)

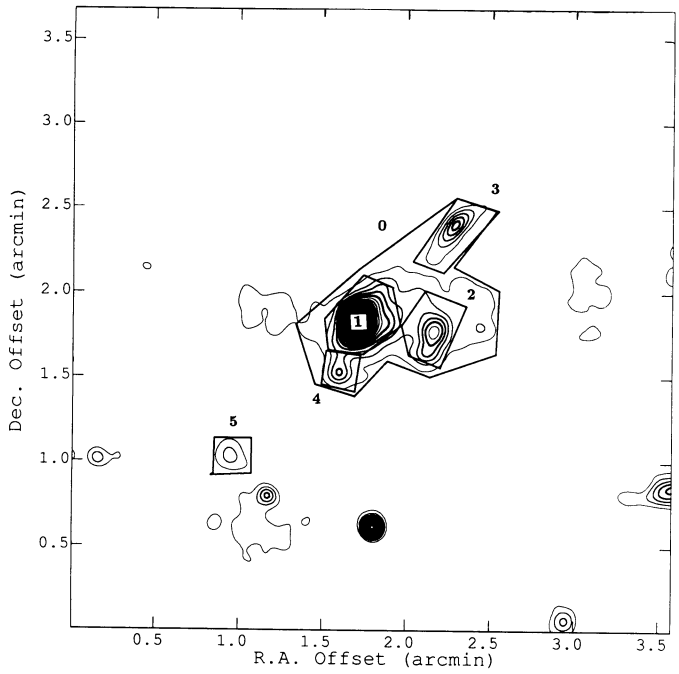

FIG. 2.—Contour map of the 2.122 μm $v = 1$–0 $S(1)$ H_2 line + continuum emission that has been degraded in resolution by convolution with a 5 pixel radius Gaussian kernel. The boxes illustrate the areas used for the flux determinations given in Table 1.

box is about 10 times the $S(1)$ line luminosity (appropriate for shock-excited gas in LTE at 2500 K; see Scoville et al. 1982), and that the observed region suffers 1 mag of extinction at 2 μm, consistent with the column density of gas derived from NH_3 and ^{13}CO observations (Bachiller et al. 1991). Estimates of the total 2.122 μm line flux and H_2 luminosity are highly uncertain due to the crude estimate of the extinction toward the emission region. In Table 1 region 0 includes regions 1 through 4, and the last column is the total emission obtained by summing regions 1 and 5.

3.1. *Comparison of* H_2 *with* CO

Figure 3 (Plate L8) shows our 2.122 μm narrow-band image of IRAS 03282+3035 superposed on velocity-integrated $J = 2$–1 CO contour maps of the outflow. Figure 3*a* shows the relationship between the extremely high velocity (EHV) gas (the molecular jet) that has a radial velocity of -57 ± -10 km s^{-1} with respect to the parent molecular cloud. Figure 3*b* shows the entire blueshifted lobe integrated from $V_{LSR} = -60$ to 0 km s^{-1} which is dominated by the low-velocity "standard high velocity" (SHV) CO flow. The registration of these images is uncertain by about 5″ due to pointing drift in the telescope and the absence of stars bright enough to use as a coordinate reference.

The peak of the molecular hydrogen emission (clump 1) lies close to the position of bullet B4 and near the northwestern edge of the region of most intense CO emission in the SHV (standard high velocity; Bachiller et al. 1991) flow. Clump 3 (the "wisp" at the top of the image) is the closest H_2 emission to the *IRAS* source. It is near the position of bullet B3. Clump 5, the faintest clump of H_2 emission, lies very close to the end of the SHV CO lobe in Figure 3*b*. No H_2 emission can be seen in the vicinity of bullets B1, B2 in the blueshifted CO lobe or from R1, R2, or R3 in the redshifted CO lobe, perhaps because of the higher extinction toward these lines of sight. Clump 2 lies close to an isolated knot of CO emission (in the EHV CO flow) that lies about 30″ west (to the right in Figs 1–3) of clump 1 (bullet B4). Figure 3 shows that there may be a close link between H_2 emission and the molecular bullets.

Bachiller et al. (1991) point out that the EHV CO appears to form a clumpy jet that "zig-zags" about the mean flow axis. The CO jet decelerates with increasing distance from the central source, terminating at the position of bullet B4 near the location of the most intense knot of H_2 emission. The low-velocity (SHV) CO emission peaks just downwind of the H_2 hot spot. Below, we argue that this morphology is consistent with a model in which a stellar jet entrains ambient CO, accelerates it, and generates the SHV CO flow in a momentum conserving interaction at the location of the shocks revealed by our H_2 observations.

4. DISCUSSION

Masson & Chernin (1993), Raga et al. (1993), and Raga & Cabrit (1993) present jet-driven models of CO outflows in which a high-velocity jet impacts undisturbed gas, accelerating it to produce the CO lobes. The impact region consists of two shocks, one moving into the undisturbed gas and one moving back into the advancing jet. The high-density layer trapped between these shocks will have a velocity intermediate between that of the jet and the surrounding medium.

CO emission may be seen from the jet in three circumstances: (1) The jet may contain CO. (2) CO and other molecules may form in shock-compressed layers (Hollenbach & McKee 1989; Neufeld & Dalgarno 1989). (3) The jet may entrain CO from the surrounding medium. The 2 μm lines of H_2 will be excited in shocks propagating into dense molecular gas with velocities in excess of 20 km s^{-1}. The highest velocity CO in the L1448 and IRAS 0328 CO jets is located between the *IRAS* source and the strongest shocks traced by H_2 emission. The apparent deceleration of the EHV CO jet and its morphology suggests that the jet entrains molecules from the cloud through which it is moving.

De Young (1986) demonstrated that two types of entrainment can occur in a jet: "*prompt entrainment*" near the "working surface" where the ram pressure of the jet sweeps up stationary gas, and "*steady-state entrainment*" along the jet walls where a turbulent mixing layer is produced by shear (Begelman & Fabian 1990; Slavin, Shull, & Begelman 1993). Deceleration of the EHV jet in IRAS 0328 may indicate that "steady-state" entrainment is occurring along the jet walls. De Young shows that for a large range of parameter space, the entrained mass is comparable to the jet mass. This mass loading may explain the presence of CO, the apparent deceleration of the EHV CO jet, and the appearance of shock-excited H_2 emission near the position of bullet B3 (clump 3), just where the jet bends to the south. In this model, the deflection of the jet produces an oblique shock in the quiescent cloud, exciting H_2 into emission, and resulting in the wispy morphology of clump 3. Shear in an oblique shock may produce turbulent mixing and mass loading that can plausibly explain the 10^{-4} $M_\odot$ clump of CO (bullet B3) as gas entrained by the jet. The nearly continuous H_2 emission that connects the bullets in the bent blueshifted lobe of L1448 (Bally et al. 1993) may also be produced in such oblique shocks.

We define the *radiative efficiency*, η, as the ratio of the corrected H_2 luminosity, $L(H_2)$, divided by the mechanical luminosity, $L_{mech} = MV^2/2\tau$, of the matter flowing through a given

1993ApJ...418L..75B

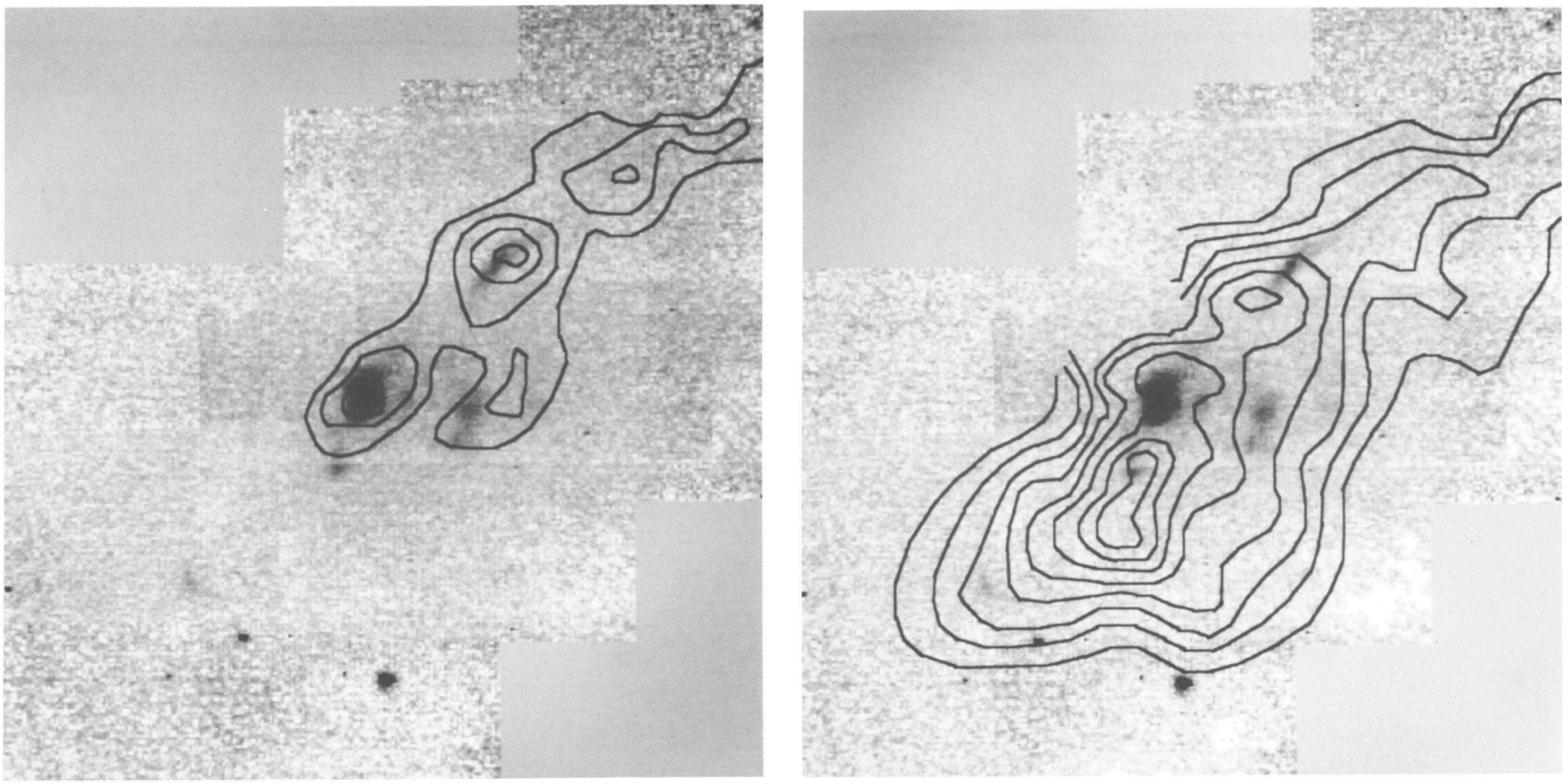

FIG. 3.—Contour map representation of the 2.122 μm $v = 1$–0 $S(1)$ H_2 line + continuum emission in the blueshifted lobe of the IRAS 0328 outflow, with contours of CO $J = 2$–1 emission superposed (taken from Bachiller et al. 1991). (*a*) Contours show the extremely high velocity CO emission in a 20 km s^{-1} wide channel centered on -57 km s^{-1} with respect to the velocity centroid of the molecular cloud. (*b*) Contours show total integrated CO emission in the blueshifted lobe between $V_{LSR} = -60$ and 0 km s^{-1}. The CO maps are taken from Bachiller et al. (1991). The registration uncertainty in the two images may be in error by up to 5″.

region. Taking the typical mass $M = 10^{-4}\ M_\odot$, the flow velocity to be $V = V_{jet}/\sin(i) \approx 90$ km s^{-1}, and the crossing time, $\tau = X/V$, where the size of the H_2 emission region is about $X \approx 8 \times 10^{16}$ cm, $\eta = 0.05$ for bullet B3, and $\eta = 0.33$ for bullet B4. The relatively low radiative efficiency of B3 compared to B4 is consistent with an oblique shock in which only a small fraction of the jet energy is radiated away. Bachiller et al. (1991) estimate that the mechanical luminosity of the entire blueshifted EHV CO flow is about 0.6 $L_\odot$. Combining this with our total estimated H_2 luminosity given in the last row in Table 1, [$L(H_2) = 0.17\ L_\odot$], gives $\eta = 0.28$ for the entire flow. The high radiative efficiency of clump 1 (bullet B4) suggests that much of the jet mechanical luminosity is converted into radiation in a strong shock at this position. CO in this region may have been accelerated by the "prompt entrainment" process. Both bullets B3 and B4 lie along the northern edge of the SHV CO lobe. This morphology and the "zig-zags" in the path of the EHV CO jet support the suggestion made by Masson & Chernin (1993) that the jet orientation may wander by about 10° in a few hundred years.

An alternative picture is that each individual clump of CO and H_2 emission represents a discrete ejection event from the YSO. The ejections from the source must be variable in both direction and in ejection velocity. This scenario does not explain in a natural way the gradual deceleration of the EHV CO jet with increasing distance from the source, nor the high H_2 luminosity of clump 1.

The large lobe of lower velocity CO emission between clump 1 and clump 5 may have been accelerated in the past when the jet was directed more toward the south. The faint knot of H_2 emission, clump 5, may be produced in a shock where the SHV CO flow collides with undisturbed cloud gas.

Our observations show that the shocks near bullet B4 consist of a group of knots separated by over 30″ from each other. At the 350 pc distance of IRAS 0328, the projected separation between knots 1 and 2 is about 1.5×10^{17} cm. If each knot corresponds to a separate working surface at the head of a jet, then the jet must have experienced extensive fragmentation or disruption.

Our observations support jet-driven lobe models for CO outflows and suggest that both "prompt" and "steady-state" entrainment might be occurring. This model, together with directional variability of the beam and breakup of the "working surface," can explain the deceleration of the EHV CO jet, the morphology of the H_2 and CO lumps, and their relationship to lower velocity CO emission. However, ejection of discrete bullets with a time variable ejection direction and velocity cannot be ruled out by our data. Further high-sensitivity observations of spectral lines which can trace the excitation of the gas and velocity-resolved spectroscopy are needed to distinguish clearly these models of CO outflow acceleration.

We thank the staff of the Apache Point Observatory for their hospitality and for making these wonderful facilities available to J. B. and D. D. The Apache Point Observatory is owned and operated by the Astrophysical Research Consortium (ARC). We thank Collin Masson, the referee, for useful comments.

REFERENCES

André, P., Martín-Pintado, J., Despois, D., & Montemerle, T. 1990, A&A, 236, 180
Aspin, C. 1992, A&A, 266, 416
Bachiller, R., & Cernicharo, J. 1986a, A&A, 166, 283
———. 1986b, A&A, 168, 262
———. 1990, A&A, 239, 276
Bachiller, R., Cernicharo, J., Martín-Pintado, J., Tafalla, M., & Lazareff, B. 1990, A&A, 231, 174
Bachiller, R., Martín-Pintado, J., & Planesas, P. 1991, A&A, 251, 639
Bally, J., Lada, E. A., & Lane, A. P. 1993, ApJ, 418, 322
Begelman, M. C., & Fabian, A. C. 1990, MNRAS, 244, 26
Borgman, J., & Blaauw, A. 1964, Bull. Astron. Netherlands, 17, 358
De Young, D. S. 1986, ApJ, 307, 62
Elias, J. H., Frogel, J. A., Matthews, K., & Neugebauer, G. 1982, AJ, 87, 1029
Garden, R. P., Russell, A. P. G., & Burton, M. G. 1990, ApJ, 354, 232
Hereld, M., Rauscher, B. J., Harper, D. A., Figer, D. F., Fischer, D., Mrozek, F., Sandford, D., & Severson, S. 1993, PASP, in preparation
Hollenbach, D., & McKee, C. 1989, ApJ, 342, 306
Margulis, M. M., et al. 1990, ApJ, 352, 615
Masson, C. R., & Chernin, L. M. 1993, ApJ, 414, 230
Masson, C. R., Mundy, L. G., & Keene, J. 1990, ApJ, 387, L47
Neufeld, D. A., & Dalgarno, A. 1989, ApJ, 344, 251
Raga, A., & Cabrit, S. 1993, preprint
Raga, A. C., Canto, J., Calvet, N., Rodriguez, L. F., & Torelles, J. M. 1993, preprint
Richer, J. S., Hills, R. E., & Padman, R. 1992, MNRAS, 254, 525
Scoville, N. Z., Hall, D. N. B., Kleinmann, S. G., & Ridgeway, S. T. 1982, ApJ, 253, 136
Slavin, J., Shull, J. M., & Begelman, M. C. 1993, ApJ, 407, 83